Desalination xxx (xxxx) xxxx

Contents lists available at ScienceDirect

Desalination

journal homepage: www.elsevier.com/locate/desal

Desalination of seawater by spray freezing in a natural draft tower

Yang Liu[a,b], Tingzhen Ming[a,c,*], Yongjia Wu[a], Renaud de Richter[d], Yueping Fang[e], Nan Zhou[c]

[a] School of Civil Engineering and Architecture, Wuhan University of Technology, Wuhan 430070, China
[b] Department of Mechatronic Engineering, Wuhan Business University, Wuhan, China
[c] China Energy Group, Environmental Energy Technologies Division, Lawrence Berkeley National Laboratory, 1 Cyclotron Road, Berkeley, CA 94720, USA
[d] Tour-Solaire.Fr, 8 Impasse des Papillons, F34090 Montpellier, France
[e] Centre for Research in the Built and Natural Environment, School of Energy, Construction and Environment, Coventry University, Priory Street, CV1 5FB Coventry, UK

ARTICLE INFO

Keywords:
Compressible airflow
Natural draft tower
Seawater desalination
Spray freezing
Water droplet

ABSTRACT

The freeze-melting process can be a viable method for the purposes of desalination because of its low energy consumption, ignorable corrosion issues, and without huge pressure or membrane replacement work. Large contact area for heat and mass transfer per unit mass of water between the water and air and low heat resistance results in higher energy efficiency during spray freezing desalination process compared to other freezing desalination methods. A 200 m high desalination tower was proposed in this paper that could generate 27.7 *kg/s* fresh water in the form of water droplets with 2 mm diameter at an atmospheric temperature of $-26^{\circ}C$. This research has founded that the natural convective airflow induced by the heat released by the warm water in the freezing process could generate through the wind turbine mounted in this system approximately one-third of the energy consumed by the water pump of the system. This free energy has never been studied in previous research. The power consumption required to produce 1 m^3 fresh water in this system is approximately 1.07 *kWh*. Compared to traditional desalination methods, the power consumption of our new spray freezing desalination system is much lower than previous systems with the same mass flow rate of fresh water. Only 375.4 *kJ* cold energy to produce one-kilogram fresh water. Thus, this spray freezing desalination system could be employed in desalination industry if free cold energy (e.g. from the cold atmosphere or the regasification process of LNG) and seawater resources are available.

1. Introduction

Water resources are unevenly distributed on the global. Shortage of affordable clear water is one of the most severe problems in many parts of the world with high population density or rapid industrialization. However, many of these areas located near to the huge water resources - seawater, for instance, Singapore, Alaska, and North China [1–3]. Low-cost and high-quality water can be exploited by desalination from the seawater to meet the urgent demand of daily consumption of a huge population and for future industrial development.

When seawater is freezing, ice tends to exclude the impurities during the crystallization process. For instance, the natural-growth sea-ice has a much lower salt content than the original seawater and is drinkable for human after it thaws. This phenomenon was found by sailors and the inhabitants living in polar regions [4]. Freeze desalination consumes less energy input by 6–7 times compared to the evaporative crystallization process due to the larger latent heat of vaporization compared to that of solidification [5]. Also, freeze desalination with no need for ancillary chemicals [4] is more environmental-friendly compared to the evaporative crystallization process. In addition, compared to the Reverse Osmosis method, the freezing melting process does not need huge pressure or membrane replacement [4,6]. Furthermore, the freeze desalination is insensitive to corrosion problems because of its low operating temperature [7]. Following the freeze desalination process, the treatments such as gravity drainage, crushing, centrifugation, filtering, washing by fresh water or even microwave treatment can further improve the quality of ice by breaking the “ice-salt pocket” in the ice and releasing the concentrated brine out of the ice [8–10]. In addition to the above advantages, the freeze-melting process will be more economic and attractive for freezing seawater if waste or renewable energy is used to freeze the seawater.

Cao et al. [11] utilized the cold (waste) energy released from the regasification process of the LNG (liquefied natural gas) by a flake ice maker to desalinate seawater, which generated 2 kg ice with 1 kg LNG re-gasification. Chang et al. [3] desalinated the seawater using the cold energy of LNG by the freezing process in Singapore. The total dissolved

* Corresponding author at: School of Civil Engineering and Architecture, Wuhan University of Technology, Wuhan 430070, China.
E-mail address: tzming@whut.edu.cn (T. Ming).

https://doi.org/10.1016/j.desal.2020.114700
Received 1 April 2020; Received in revised form 30 July 2020; Accepted 8 August 2020

Nomenclature

A	Heat (mass) transfer area per tower unit volume (m^2/m^3)
A_d	Surface area of a water droplet (m^2)
Bi	Biot number
C_d	Drag coefficient
$C_{p,\ B}$	Specific heat capacity of dry air (J/kg·K)
$C_{p,\ w}^{\ g}$	Specific heat capacity of water vapor (J/kg·K)
$C_{p,\ w}^{\ L}$	Specific heat capacity of liquid water (J/kg·K)
d	Diameter of a water droplet (m)
D	Diameter of the tower (m)
$D_{w,\ a}$	Diffusivity of water vapor in air (m^2/s)
fr_{ice}	Ice mass fraction
F	Force (N)
F_r	Froude number
g	Gravitational acceleration, 9.81 (m/s^2)
G_B	Mass flow rate of dry air per unit cross-section area (kg/m^2·s)
h	Tower height (m)
h_{conv}	Convective heat transfer coefficient (W/m^2· K)
h_{mass}	Mass transfer coefficient (kg/s·m^2·(kg/kg)$^{-1}$)
H_d	Specific enthalpy of a droplet (J/kg)
H_G	Specific enthalpy of moist air per unit mass of dry air (J/kg)
ΔH_s	Specific latent heat of fusion (J/kg)
H_w	Specific enthalpy of the liquid phase (J/kg)
ΔH_v	Specific heat of vaporization of water (J/kg)
k	Thermal diffusivity (W/m · ° C)
L	Mass flowrate of water per unit cross-section area (kg/m^2·s)
M	Mach number
M_a	Molar mass of moist air (kg/kmol)
m_d	Mass of a water droplet (kg)
m_w	Mass flow rate of the feed water (kg/s)
N	Number of water drops falling through a unit volume per second
Nu	Nusselt number
P	Air static pressure (Pa)
P_r	Prandtl number
$P_{w,\ sat}$	Vapor pressure of the seawater (Pa)
q	Heat-transfer flux (w/m^2)
Q	Heat transferred per unit mass (w/kg)
R	Specific gas constant for air, 287 (J/kg·K)
R_e	Reynolds number
S	Cross-section area of the tower (m^2)
S_c	Schmidt number
S_h	Sherwood number
t	Time (s)
T	Temperature (K)
v	Velocity (m/s)
Y_w	Humidity mass ratio of moist air (kg/kg)
$Y_{w,\ i}$	Humidity mass ratio at the gas-phase side of interface (kg/kg)
z	Height from the bottom of the tower (m)

Greek symbols

α	Thermal diffusivity (m^2/s)
γ	Specific heat ratio of air
ε	Pressure loss coefficient
ζ	Turbine pressure drop factor
η	Mechanical efficiency of turbine generator
λ	Friction coefficient on the wall in the tower
ρ	Air density (kg/m^3)
μ	Dynamic viscosity ($P_a \cdot s$)
Δ	Difference

Subscripts

a	air
b	buoyancy
br	internal bracing
d	droplet
da	dry air
f	freezing point
g	gravitational
in	inlet
ice	ice
k	kinetic energy
la	lapse rate
loss	loss
n	nucleation
out	outlet
pot	potential
tur	turbine
w	water
∞	atmosphere
0	sea level

Shorthand with no physical meaning

MX
EX
EXw

solids at around 300 ppm were achieved by washing in the final product, which meets the salinity of 500 ppm of WHO potable water standard. Wang and Chung [12] developed a hybrid desalination process comprising freeze desalination (cold energy from LNG) and membrane distillation processes. High-quality drinkable water with a low salinity of 0.104 g/L was obtained in the freeze desalination process alone. Combined with freeze desalination, the membrane distillation process was employed to treat the brine discharged from the freeze desalination unit. Drinkable clean water was successfully produced by the hybrid process with a total water recovery of 71.5%. John et al. [13] even proposed to purify the urban wastewater by the natural freeze. With this method, no cold energy input was needed and 95% purification efficiency was achieved. Once free cold energy is available, there is potential to generate clear water by the freeze desalination method.

Some devices were specially designed for crystallizing the salt solution to generate ice and solid salt simultaneously. A novel 151 freezing disk column crystallizer has been built to separate the frozen salt solution into ice and salt under the eutectic freezing point [14]. With this device, as a case study, a 35 w% aqueous sodium nitrate and a 12 w% copper sulfate stream fed into the disk column crystallizer were cooled down to the eutectic freezing point to separate water and salt. Compared to conventional multi-step evaporation, the energy reductions by using freeze desalination are 30% of that of sodium nitrate and 65% of that of copper sulfate [15].

Although it has been demonstrated that the freeze-melting process could be a method for desalination, the block, layer, or falling film freeze processes are not energy-efficient. Large thermal resistance exists due to the wall of the heat exchanger, the water, or the ice itself, which results in a low rate of heat transfer and long crystallization time. So, a direct freezing method - spray freezing with a large area of heat transfer with a low thermal resistance is preferred in the freeze-melting process.

During the spray freezing process, the water droplets are sprayed directly into the cold air to be frozen. The large surface area per unit volume of water drops makes the rates of both cooling and ice formation much faster.

When the seawater is pumped and sprayed into the cold air, the surface temperature of water droplets falls below ice nucleation temperature, they solidify from the outside and push the impurities to the center of the drop by crystallization front, resulting in a higher concentrated liquid and nearly pure ice [16]. The outer shell fracture, when droplets fall and contact with the cold ground. The built-up pressure inside the droplet caused by phase change expansion can also rupture the ice shell, and release the liquid impurities out of the droplet [17]. The excess water drained out from a spray ice deposit becomes runoff that is more concentrated than the original seawater.

The spray freezing process was proposed to produce drinkable water in Alaska in the 1960s, which achieved salt concentration in the ice 0.007 times lower than the source seawater [2]. The spray freezing was also used to treat pulp mill effluent and oil sands tailings pond water by Gao et al. [18]. In Gao's experiment, greater than 60% impurity reduction in the spray ice was obtained when 30% of the total volume of the sprayed water was released as runoff. Another field experiment was conducted to evaluate the efficiency of spray freezing to remove dissolved chemicals from the lake of tailing water at the Colomac Mine. The experimental analysis showed that after the initial 39% of the spray ice column had been melted, the efficiency of dissolved chemical removal in the ice core reached up to 87–99% [19]. Tatarniuk et al. [20] used spray freeze separation to concentrate salt in snowmelt water gathered from snow runoff water on the roads into higher concentrated reusable brine to recover and recycle salts, intending to drive down salt costs in the Canadian winter. The spray freezing could concentrate the water 1.3– 1.4 times higher than the source water, with much purer ice mound left.

Although the spray freezing to purify water is proved to be feasible, a large-scale continuously-running spray freezing system has not been proposed. The heat and mass transfer mechanism during the spray freezing and the impact factors in this spray freezing process have not been analyzed yet. Besides, in a large-scale continuously-running spray freezing system, the heat energy released from the water droplets during its freezing was never utilized in the previous research. Actually, this energy is a kind of heat that could heat the cold air and form natural air current which can be utilized in a spray freezing tower to propel the turbines mounted on the top of the tower to generate electricity (see Fig. 1). So, the main objective of this paper is to desalinate seawater by spray freezing utilizing the free cold energy from the atmosphere (or from LNG) and generate green power simultaneously. An economic analysis of this method compared with freezing by a heat-exchanger is also undertaken in this paper.

2. Principle of the spray freezing desalination

To freeze the sprayed seawater droplets and utilize the free heat energy released by the water, a 200 m high spraying tower with turbines mounted at the bottom is introduced in this paper. The warm seawater droplets are sprayed from the top of the tower, the freely-falling droplets would release heat into the air inside the tower. The heated air in the tower would float upwards because of its lower density, which caused a natural air draft. The updraft can be used to propel the turbines to generate electricity.

At the upper part of the tower, the droplets will be in the liquid state. When the temperature of droplets reduces to the freezing temperature, they will be frozen and become ice particles. If the droplets are partially frozen, the mixture of ice and concentrated brine is collected by the ice container at the bottom and filtered. Pure ice will be separated from brine and stored to produce fresh water. The concentrated brine will drain off. This proposed spray freezing desalination is presented in Fig. 1. The geometrical parameters of this system are derived from [21].

The principle of desalination by freeze crystallization can be described by the typical phase diagram of binary solution which represents the equilibrium lines between solid and liquid states of materials. A schematic representation of the phase change diagram of saline water (NaCl-H_2O) is depicted in Fig. 2. Line 1 defines the freezing point of water at different sodium chloride mass content.

The starting point is on the left side of the eutectic point when the mass fraction is lower than 23.3 wt%. The unsaturated saline solution is cooled until reaching the equilibrium point on Line 1. Further cooling will take the solution along Line 1 with equilibrium temperature depressing and concentration in remain liquid increasing until the eutectic point is reached at $-21.1\ ^{\circ}C$ for NaCl solution.

The freezing point depression, T_f, depends linearly on the concentration of the salt and can be calculated as [23]:

$$T_f = -54.1126\left(\frac{S_w}{1-S_w}\right),\ -7.7 \le T_a \le 0°C\ and\ 0 \le S_w \le 12.47\% \quad (1)$$

where S_w is the salinity of the seawater (0.035 for the initial salinity before desalination).

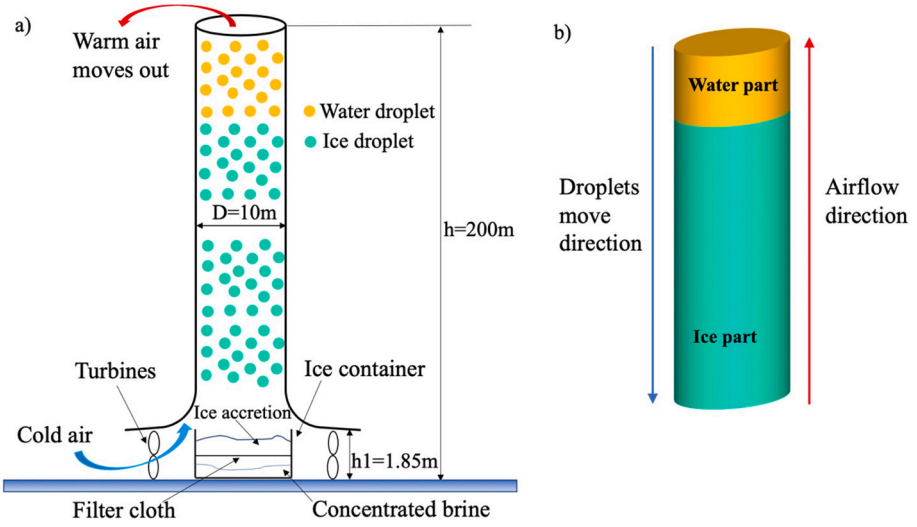

Fig. 1. (a) Schematic diagram of the spray freezing desalination system, (b) flow directions of seawater droplets and air.

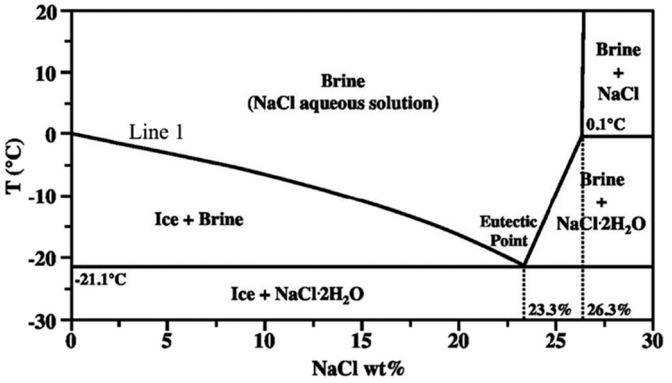

Fig. 2. Phase diagram for the NaCl solution as a function of temperature and salt concentration [22].

3. A single water droplet freezes in the tower

3.1. A single water droplet velocity

As the heat and mass transfer rate between the water droplets and the surrounding air is decided by the drops' velocity, the velocity of the drops must be analyzed first. In this work, the water drops were assumed to be spherical [24] and fall vertically in the one-dimensional model. The forces exerted on one droplet include gravity F_g, buoyancy from the air F_b, air friction drag F_a. The force balance equation is:

$$m_d \frac{dv_w}{dt} = F_g - F_b - F_a \tag{2}$$

where v_w= velocity of a water droplet, t = time (s).

The mass of a water droplet m_d can be calculated by $m_d = \pi d^3 \rho_w/6$, the gravitational force of a droplet is $F_g = \pi d^3 g \rho_w/6$ and the buoyancy is $F_b = \pi d^3 g \rho_a/6$. The drag force by air friction F_a is expressed as $F_a = \pi C_d \rho_a (v_a + v_w)^2 d^2/8$. The $\rho_w$and ρ_a represent the density of water and air, respectively. Then the motion equation of the water droplet can be written as [25]:

$$\frac{dv_w}{dt} = g\left(1 - \frac{\rho_a}{\rho_w}\right) - \frac{3}{4}\frac{C_d}{d}\frac{\rho_a}{\rho_w}(v_a + v_w)^2 \tag{3}$$

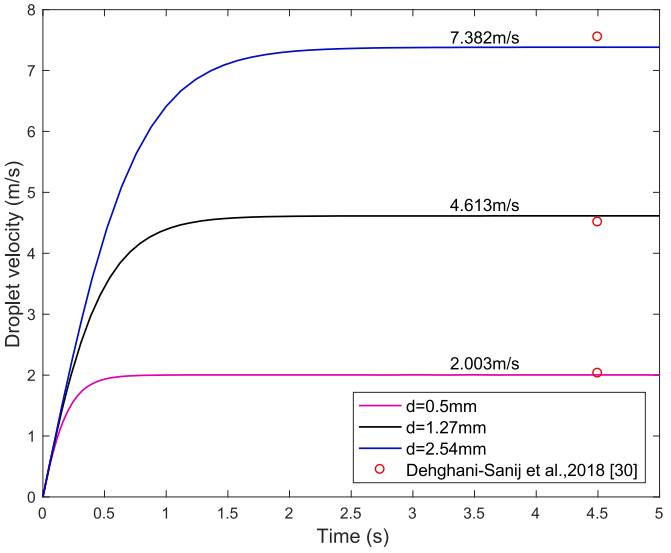

Fig. 3. The freely-falling droplet velocity variation after the release in the static air.

For liquid droplets, the following drag coefficient correlations were adopted [26]:

$$C_d = \begin{cases} \dfrac{24.0}{\mathrm{Re}}, & \mathrm{Re} \le 1 \\ \dfrac{24.0}{\mathrm{Re}}(1 + 0.15\mathrm{Re}^{0.687}), & 1 < \mathrm{Re} \le 1000 \\ 0.44, & \mathrm{Re} > 1000 \end{cases} \tag{4}$$

where R_e is the Reynolds number, $R_e = \rho_a(v_a + v_w)d/\mu_a$.

The thermophysical properties of seawater and air needed for the numerical calculation are listed in Table 1.

By solving Eq. (3), the free-falling droplet velocity variation from the release in the static air is shown in Fig. 3 (the variation of v_a is discussed in Section 4 in this paper). Larger droplets tend to have a higher terminal velocity. The small differences in droplet velocity between the present model and the model of Dehghani-Sanij et al. [30] are due to the different C_d estimation. The velocity variations are in good agreement with the experimental results conducted by

Table 1
Parameter quantities and correlations used.

Parameter	Quantity/correlation	Units	References
S_w	35	g/kg	[27]
T_f[1,2]	$-54.1126\left(\frac{S_w}{1-S_w}\right)$	$^\circ C$	[23]
ρ_w	$1000 + 0.8S_w$	kg/m^3	[23]
$C_{p,w}^{L}$	$1.005 - 0.004136S_w + 0.0001098S_w^2 - 0.000001324S_w^3$	$Cal/g \cdot ^\circ C$	[23]
ΔH_v[3]	2,498,510 ($0\ ^\circ C$, *salinity* 3.5%)	J/kg	[27]
ΔH_s[3]	329,928 (*salinity* 3.5%)	J/kg	[27]
$P_{w,sat}$[3]	602.4 ($0\ ^\circ C$, *salinity* 3.5%)	P_a	[27]
ρ_a	$\frac{P \cdot M_a}{8.3145 \times 10^3 T_a}$	kg/m^3	[28,29]
M_a	$(1 + Y_w)/\left(\frac{Y_w}{18.015} + \frac{1}{28.966}\right)$	$kg/kmol$	[28,29]
$D_{w,a}$	$2.227 \times 10^{-5}\left(\frac{T_a + 273.15}{273.15}\right)^{1.81}$	m^2/s	[23,29]
μ_a	$\mu_0\left[\frac{416.16}{T_a + 393.15}\left(\frac{T_a + 273.15}{296.16}\right)^{1.5}\right]$ $\mu_0 = 1.8325 \times 10^{-5} P_a \cdot s$	$P_a \cdot s$	[23]
α_a	$\frac{1}{(57736 - 585.78T_a)}$	m^2/s	[23,29]
κ_a	$0.024577 + 9.027 \times 10^{-5} T_a$	$W/m \cdot ^\circ C$	[23,29]

[1]The equation is valid in $-7.7 \le T_a \le 0\ ^\circ C$ *and* $0 \le S_w \le 12.47\%$.
[2]The salinity, S_w, appears as a fraction in this formula (0.035 for Standard Ocean salinity).
[3]The accurate data is available from http://www.teos-10.org.

Chowdhury et al. [31]. The experiment demonstrated that velocity of water drops grew very rapidly at the beginning and reached to the peak (terminal) velocity after a very short time period and distance. When the droplets reaching the peak (terminal) velocity, they no longer accelerate and keep at this velocity constantly. The terminal velocities of falling water droplets in the air are also demonstrated by many researchers in their experiments [32–34].

3.2. A single water droplet freezing process

During the freezing process, the temperature inside of a droplet, in general, varies with time and the position. To simplify and solve the transient heat transfer phenomenon of water droplet, the Biot number, which is the ratio of heat convection at the surface to the internal heat conduction of a body, is first evaluated.

$$Bi = \frac{h_{conv}\frac{d}{6}}{k_d} \tag{5}$$

where the h_{conv} is the convection heat transfer coefficient and the k_d is the droplet (water or ice) thermal conductivity. A small Bi represents lower resistance to conduction within a body. For $Bi < 0.1$, the temperature gradient within the droplet can be neglected and uniform temperature within the body is regarded for the droplet.

One may notice that the Bi number would be slightly larger than 0.1 before the phase change stage when the water droplet diameter is larger than 2.5 mm. However, in the calculation of Bi number, the circulation and mixing inside a freely falling water droplet, which could enhance internal heat transfer within a body, is not considered yet. The Reynolds number of the internal motion within a droplet is defined as [17,35]:

$$Re_{int} = \frac{v_a d}{2\left(1 + \frac{\mu_w}{\mu_a}\right)\frac{\mu_w}{\rho_w}} \tag{6}$$

where μ_w and μ_a is the dynamic viscosity of droplet and air, respectively.

Considering the internal motion, the effective thermal diffusivity is expressed as [17,35]:

$$\alpha_{w,eff} = \frac{k_w}{\rho_w C_{p,w}^L} = \alpha_w(1 + 0.01Re_{int}) \tag{7}$$

The $\alpha_{w,\ eff}$ is more than 10 times larger than the α_w of non-internal-motion seawater, which means that the effective thermal conductivity k_w is much larger. Thus, even if the water droplet is bigger than 2.5 mm, the Bi number is still smaller than 0.1 if the internal motion within the droplet is considered. Furthermore, the thermal conductivity of ice is about four times larger than that of seawater α_w, the Bi number is still smaller than 0.1 when the ice is formed. Hindmarsh et al. [36] also demonstrated that a simple heat balance model is sufficient for the purpose of solving the internal energy balance of the droplet, giving accurate results. Therefore, the temperature gradient within the droplet is neglected in the whole freezing process of a droplet in this paper and a simple heat balance model was used.

The freezing process of a droplet can be divided into four stages: initial (liquid) supercooling, recalescence, solidification (phase change), and post-solidification (solid) stage [36,37]. The theory was based on that the liquid droplet will not crystallize until it is supercooled and reaches the nucleation temperature T_n which is much lower than the freezing temperature T_f. Once the first crystal nuclei are formed, a rapid crystallization happens, resulting in a sudden temperature rise from T_n to T_f, which is called the recalescence stage.

The droplet continuously releases heat during its freezing process, the total energy released includes the convective heat loss, radiative heat loss, and evaporative heat loss:

$$q_{total} = q_{conv} + q_{rad} + q_{evap} \tag{8}$$

$$q_{conv} = h_{conv}(T_d - T_a) \tag{9}$$

$$q_{rad} = \varepsilon\sigma(T_d^4 - T_a^4) \tag{10}$$

$$q_{evap} = h_{mass}(Y_{w,i} - Y_w)\Delta H_v \tag{11}$$

$$Y_{w,i} = 0.622\frac{P_{w,sat}}{P - P_{w,sat}} \tag{12}$$

where the T_d is droplet (water or ice) temperature, T_a is the atmosphere temperature, σ is the Stefan-Boltzmann constant, ε is the droplet emissivity. $Y_{w,\ i}$ is the humidity mass ratio of saturated moist air at the water-air interface, which depends on the droplet temperature T_d. Y_w is the humidity mass ratio of moist atmospheric air.

The convective heat and mass transfer coefficient h_{conv} and k_{mass} were obtained from experimental data by Ranz and Marshall [38]:

$$N_u = \frac{h_{conv}d}{k_a} = 2 + 0.6P_r^{1/3}R_e^{1/2} \tag{13}$$

$$S_h = \frac{h_{mass}d}{D_{w,a}} = 2 + 0.6S_c^{1/3}R_e^{1/2} \tag{14}$$

where N_u is Nusselt number, P_r is Prandtl number $P_r = \mu_a/\rho_a\alpha_a$, S_h is Sherwood number, S_c is Schmidt number $S_c = \mu_a/\rho_a D_{w,\ a}$, R_e is the Reynolds number.

Due to the mass transfer, the droplet mass decreases continuously until the evaporation ends. The mass change of a droplet can be calculated by:

$$(m_d)_t = h_{mass}(Y_{w,i} - Y_w)A_d\Delta t + (m_d)_{t+\Delta t} \tag{15}$$

$$\frac{dm_d}{dt} = -h_{mass}(Y_{w,i} - Y_w)A_d \tag{16}$$

where m_d is the mass of a water droplet and the A_d is the surface area of a water droplet.

According to [16], when a droplet surface temperature reaches the freezing point, ice nucleation begins at the surface, a solid shell grows rapidly around the surface (about 2/30–3/30 s) and then solidifies inwards. The evaporative mass transfer from the water to the ambient air can be neglected during the ice formation process around the droplet surface.

Before the solidification (phase change) stage, the energy balance for the droplet is:

$$(m_d H_d)_t = (m_d H_d)_{t+\Delta t} + A_d q_{conv}\Delta t + A_d q_{rad}\Delta t + A_d q_{evap}\Delta t \tag{17}$$

and the final expression for the water temperature T_d is

$$\frac{dT_d}{dt} = -\frac{h_{conv}A_d(T_d - T_a) + \varepsilon\sigma(T_d^4 - T_a^4)A_d + h_{mass}(Y_{w,i} - Y_w)A_d\Delta H_v}{m_d C_{p,w}^L} \tag{18}$$

During the solidification (phase change) stage, the ice is formed from the outside and it pushes the impurities to the center of the drop, resulting in a higher concentrated liquid and nearly pure ice. This concentrated solution would decrease the freezing temperature until the new equilibrium is reached. Thus, the heat released by the droplet will not only facilitate the phase change but also reduce the droplet (both the outside ice and the inside concentrated solution) temperature. Since the diffusion of impurities in the ice can be negligible [37,39], the droplet temperature will follow the freezing point depression line (see Fig. 2). Based on this theory, the energy balance for the droplet is:

$$(m_d H_d)_t = (m_d H_d)_{t+\Delta t} + A_d q_{conv}\Delta t + A_d q_{rad}\Delta t - \Delta H_s m_d fr_{ice} \tag{19}$$

and the final expression is:

$$\Delta H_s m_d \frac{df_{r_{ice}}}{dt} - (C_{p,ice} m_d f_{r_{ice}} + C_{p,w}^L m_d (1 - f_{r_{ice}})) \frac{dT_d}{dt} = A_d q_{conv} + A_d q_{rad} \tag{20}$$

where fr_{ice} is the ice mass fraction in the droplet, ΔH_s is the specific latent heat of fusion.

Eq. (19) could be solved with the freezing point depression equation (Eq. (1) for seawater) with a forward difference time step method [37] or a chain rule method [39]:

$$\frac{dT_d}{dt} = \frac{dT_d}{df_{r_{ice}}} \frac{df_{r_{ice}}}{dt} = \frac{dT_f}{df_{r_{ice}}} \frac{df_{r_{ice}}}{dt} \tag{21}$$

For seawater, when the ice appears, the freezing point could be expressed as:

$$T_f = -54.1126 \left(\frac{S_w/(1 - f_{r_{ice}})}{1 - S_w/(1 - f_{r_{ice}})} \right) \tag{22}$$

where S_w is the initial salinity of the seawater before crystallization.

The phase change stage ends when the temperature of the droplet or the concentration of the inside solute reaches the eutectic point (23.3% for seawater). After that the post- solidification stage starts. The droplet temperature can be expressed as:

$$\frac{dT_d}{dt} = -\frac{h_{conv} A_d (T_d - T_a) + \varepsilon\sigma (T_d^4 - T_a^4) A_d}{C_{p,ice} m_d f_{r_{ice}} + C_{p,w}^L m_d (1 - f_{r_{ice}})} \tag{23}$$

To validate this numerical model, the freezing process of a sucrose droplet was simulated. The comparison with the reference [39,40] was made in Fig. 4. In [39], the temperature variation of a solution droplet during the freezing process was discussed. The solute mass fraction was analyzed in the following paper [40]. The boundary conditions were: $T_a = -15\ ^\circ C$, $d = 1.56mm$, $v_a = 0.42m/s$, $v_w = 0m/s$. A slight difference between the model in the reference [39,40] with the present model was observed in this figure. In [39,40] the temperature gradient of the surface ice was considered and the inside concentrated solution was treated as a lumped matter. Thus, $C_{p,\ ice} m_d f_{r_{ice}}$ in Eq. (20) was not calculated in those papers (see Eq. (20) in [39]). While, in this paper, as discussed before, the temperature gradient of the droplet (ice/water) was neglected, since the thermal conductivity of ice is about four times larger than the seawater. The protuberance of the solute mass fraction at the beginning of the freezing process (between 4.5 and 5 s) was caused by the ice formed in the recalescence stage.

4. A system of droplets freeze in the tower

4.1. Collision and coalescence of water droplets

As discussed in the previous section, since the large droplets will reach a higher terminal velocity than that of the smaller droplets. When different diameters of water droplets are emitted by a spray nozzle, the larger droplets will collide with the smaller ones during the falling process in the tower. Some of the smaller droplets will be collected by the larger ones after the collision and resulting in coalescence. Those droplets collided without a coalescence will bounce away from each other. The probability of coalescence depends on the collision angle of two droplets [41].

The concept of Energy Tower that cools the hot desert air by spraying seawater on the top of the tower and thus generates a downdraft to produce power was proposed by [41]. In this paper, the collision frequency between two droplets with different velocity was expressed as:

$$\Theta = N_1 N_2 \pi (d_1/2 + d_2/2)^2 |v_{w,1} - v_{w,2}| \tag{24}$$

where N is the number of droplets per unit volume, d is the droplet diameter, and the subscript 1 and 2 indicate different diameters of the droplets. The probability of coalescence is set to be 1/2. In this energy tower, the calculation indicates that the model with collision consideration produced only 6% lesser energy (or the velocity of the downdraft) in this 1000 m-high tower compared with no collision consideration.

To simplify the mathematical process, the so-defined Sauter diameter was proposed by Makkinejad [42] to replace all the droplets with different sizes by a population of spherical uniform-size droplets in the tower (thus no collision would happen). The equalized spherical droplet diameter is $d_s = \sum_i d_i^3 / \sum_i d_i^2$. It was found that this model produces small deviations ($< 2.1\%$) in an industrial counter cooling tower. Therefore, a population of spherical uniform-size drops was assumed in the following section.

4.2. Heat and mass transfer between water droplets and air

Assumptions listed below are also suggested in this article:

1) The process is under the steady-state, which means the variables of the process are unchanging in time under a given condition. The initial situation (a transient state or a start-up period) is not considered;
2) One-dimensional compressible flow in the tower without crosswind;
3) The distribution of water and air mass flow is uniform inside the tower;

Since the freezing process of seawater can be divided into four stages, the tower will also be separated into sections to calculate the parameters of the air. But it should be noticed that the recalescence stage will not happen in the freely falling seawater droplets because the nucleation temperature is slightly higher (0.3%–0.4%) than the freezing temperature [17]. Then the tower is divided into two parts: i) in the upper part, the water droplets still stay above the freezing point. Heat and mass transfer happen simultaneously in this part; ii) in the lower part, because of the solid shell, the mass transfer from the water to the ambient air can be neglected when the ice is formed quickly around the surface.

Llano-Restrepo [28] proposed a set of equations to numerically calculate the heat and mass transfer between water and air in a spray cooling tower neglecting the radiative heat transfer. Those equations transform the temperature gradient against the time (s) to against z (m) by introducing L and A to substitute the m_d and A_d, respectively. In the following equations, z is the vertical distance from the bottom of a cooling tower upward, G_B is the mass flow rate of dry air per unit cross-section area of the cooling tower ($kg/m^2 \cdot s$), L is the water mass flow rate per unit cross-section area of the cooling tower $kg/m^2 \cdot s$, A is the

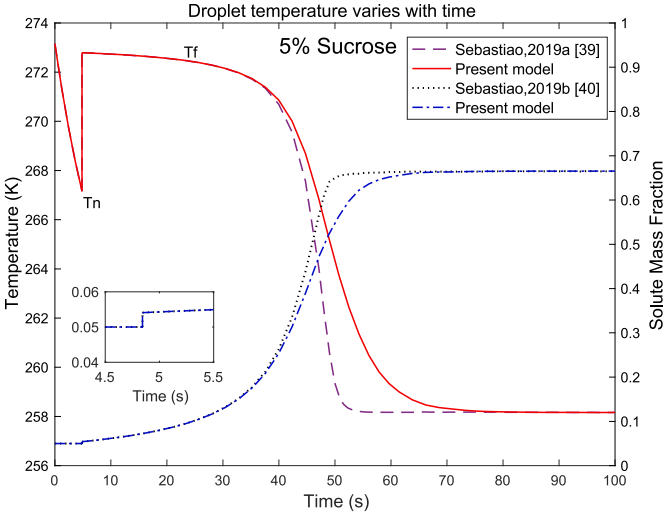

Fig. 4. The freezing process of a 5% sucrose droplet.

interfacial area per tower unit volume (m^2/m^3), $A = N \cdot \pi d^2$, and N is the number of water drops falling through a unit volume per second, $N = 6L/\rho_w \pi v_w d^3$. With the addition of the radiative heat transfer, those equations were given below, a more comprehensive analysis can be found in [28]:

for the humidity mass ratio, Y_w is:

$$\frac{dY_w}{dz} = h_{mass}(Y_{w,i} - Y_w)A/G_B \tag{25}$$

for the water mass flow rate, L is

$$\frac{dL}{dz} = h_{mass}(Y_{w,i} - Y_w)A \tag{26}$$

for the air temperature, T_a is

$$\frac{dT_a}{dz} = \frac{h_{conv}A(T_w - T_a) + +\varepsilon\sigma(T_w{}^4 - T_a{}^4)A + h_{mass}(Y_{w,i} - Y_w)A\int_{T_a}^{T_w} C_{p,w}^g dT}{G_B(C_{p,B} + Y_w C_{p,w}^g)} \tag{27}$$

for the water temperature, T_L is

$$\frac{dT_w}{dz} = \frac{h_{conv}A(T_w - T_a) + \varepsilon\sigma(T_w{}^4 - T_a{}^4)A + h_{mass}(Y_{w,i} - Y_w)A\Delta H_v}{LC_{p,w}^L} \tag{28}$$

Eqs. (25), (26) and (28) can be used for water droplets before the phase change stage in the tower (it should be noticed that the minus sign was not shown in Eqs. (26) and (28) because of the differential direction). During the phase change stage, one can easily transform Eqs. (19)–(21) from $\frac{dT_w}{dt}$ to $\frac{dT_w}{dz}$. But the Eq. (27) that treated the air as incompressible gas without considering the variations of air density and air pressure in the cooling tower is not suitable for the model in this paper, because the continuous density change of air in this model is the main reason for the formation of natural draught during the seawater droplets freezing. And the volume of airflow dominates the maximum quantity of seawater that can be frozen in the tower (see the Results and discussion section).

To solve the one-dimensional compressible airflow in a high tower, a method for calculating this buoyant flow induced by the variation of air density was proposed in [43], validated by [44] and further developed by [45]. But the forces that coupling between discrete water droplets and continuous air were not considered in those models, which are not neglected in the model of this paper. The new method considering the forces from water droplets and the heat/mass transfer between water and air is expressed into two parts according to the freezing stage of the droplets:

1) During the phase change stage of the seawater droplets:

The state equation of air:

$$\frac{dP}{P} - \frac{d\rho_a}{\rho_a} - \frac{dT_a}{T_a} = 0 \tag{29}$$

The continuity equation of air after the water droplets fell below freezing temperature:

$$d(\rho_a v_a S) = 0 \Rightarrow \frac{d\rho_a}{\rho_a} + \frac{dv_a}{v_a} = 0 \tag{30}$$

The momentum equation of air:

$$dP + \rho_a v_a dv_a + \rho_a g dz + \frac{\lambda}{D}\bullet\frac{\rho_a v_a{}^2}{2}\bullet dz + F_w dz = 0 \tag{31}$$

where λ is the friction coefficient on the wall of the tower, $\lambda = 0.008428$ [43],

F_w is the source term of momentum due to the forces of water droplets.

The F_w was given in [46] as:

$$F_w dz = \frac{dv_w}{dt}\frac{m_w dt}{d\forall}dz = \frac{dv_w}{dt}\frac{L\bullet S\bullet dt}{d\forall}dz = \frac{dv_w}{dt}\frac{L}{dz/dt}dz = \frac{dv_w}{dt}\frac{L}{v_w + v_a}dz \tag{32}$$

where m_w is the water mass flow rate kg/s, $d\forall$ is the control volume, S is the cross-section area of the tower m^2.

To solve those equations, two more numbers were introduced:

Mach number is defined as the ratio of local velocity v and the speed of sound:

$$M = \frac{v_a}{\sqrt{\gamma RT}} \tag{33}$$

where γ is the specific heat ratio of air, $\gamma = C_{p,\,a}/C_{v,\,a}$.

Froude number is defined as the ratio between inertial and gravity force:

$$F_r = \frac{v_a}{\sqrt{gD}} \tag{34}$$

This momentum equation can be expressed finally as:

$$\frac{dP}{P} + \gamma M^2\frac{dv_a}{v_a} = -\gamma M^2\bullet\frac{2}{\lambda F^2}\bullet\frac{\lambda}{2D}dz - \gamma M^2\bullet\frac{\lambda}{2D}dz - \frac{F_w dz}{P} \tag{35}$$

To make the formulae read easily, a shorthand for the right-hand side of Eq. (35) is introduced as MoX.

The energy equation of air per unit mass:

$$dW - dQ + dH + v_a dv_a + g dz = 0 \tag{36}$$

where W is the work, Q is the heat transferred during the height of dz, H is the enthalpy.

Since the work is zero, this equation can be rewritten as:

$$C_p dT_a + v_a dv_a + g dz = dQ \tag{37}$$

With neglecting mass transfer:

$$dQ = dQ_{ice} = \frac{[q_{conv} + q_{rad}]A - \pi D q_{wal}}{G_B}dz \tag{38}$$

where dQ_{ice} is heat transferred from water droplets during the phase change stage.

q_{wal} is the heat loss of the air through the tower wall and can be expressed as [47]:

$$q_{wal} = h_{wal}(T_a - T_{z,\infty}) \tag{39}$$

$$Nu_{wal} = \frac{h_{wal}D}{k_a} = 0.023P_r{}^{0.3}R_e{}^{0.8} \tag{40}$$

where h_{wal} is the heat transfer coefficient, and $T_{z,\,\infty}$ is the temperature of the atmosphere at the height z.

This energy equation can be expressed finally as:

$$\frac{\gamma}{\gamma - 1}\bullet\frac{dT_a}{T_a} - \frac{dP}{P} = \gamma M^2\bullet\frac{\lambda}{2D}dz + \frac{F_w dz}{P} + \frac{\rho_a dQ_{ice}}{P} \tag{41}$$

To make the formulae read easily, a shorthand for the right-hand side of Eq. (41) is introduced as EX.

After solving Eqs. (29), (30), (35), and (41) above, we get:

$$\frac{dT_a}{T_a} = \frac{\gamma - 1}{\gamma(M^2 - 1)} \bullet [(\gamma M^2 - 1) \bullet EX - MoX] \tag{42}$$

$$\frac{dv_a}{v_a} = \frac{1}{\gamma(M^2 - 1)} \bullet [MoX - (\gamma - 1) \bullet EX] = -\frac{d\rho_a}{\rho_a} \tag{43}$$

$$\frac{dP}{P} = \frac{\gamma - 1}{M^2 - 1} \bullet [M^2 \bullet EX - MoX/(\gamma - 1)] \tag{44}$$

$\frac{dT_a}{dz}$, $\frac{dv_a}{dz}$,and $\frac{dP}{dz}$ can be calculated from Eqs. (42), (43) and (44).

2) When the water droplets are still above freezing temperature, the continuity equation of air can be rewritten as:

$$d(\rho_a v_a) = dL \Rightarrow \frac{d\rho_a}{\rho_a} + \frac{dv_a}{v_a} = \frac{dL}{\rho_a v_a} = \frac{h_{mass} A (Y_{w,i} - Y_w)}{\rho_a v_a} dz \tag{45}$$

The energy equation is:

$$\frac{\gamma}{\gamma - 1} \bullet \frac{dT_a}{T_a} - \frac{dP}{P} = \gamma M^2 \bullet \frac{\lambda}{2D} dz + \frac{F_w dz}{P} + \frac{\rho_a dQ_w}{P} \tag{46}$$

$$dQ_w = \frac{A[q_{conv} + q_{rad} + q_{evap}] - \pi D q_{wal}}{G_B} dz \tag{47}$$

where dQ_w is heat transferred from water when water stayed above freezing temperature.

To make the formulae read easily, a shorthand for the right-hand side of Eq. (46) is introduced as EXw.

After solving Eqs. (29), (35), (45) and (46) above, we get:

$$\frac{dT_a}{T_a} = \frac{\gamma - 1}{\gamma(M^2 - 1)} \bullet \left[(\gamma M^2 - 1) \bullet \left(EXw + \frac{dL}{\rho_a v_a} \right) - \left(MoX - \frac{dL}{\rho_a v_a} \right) \right] \tag{48}$$

$$\frac{dv_a}{v_a} = \frac{1}{\gamma(M^2 - 1)} \bullet \left[\left(MoX - \frac{dL}{\rho_a v_a} \right) - (\gamma - 1) \bullet \left(EXw + \frac{dL}{\rho_a v_a} \right) \right] \tag{49}$$

$$\frac{dP}{P} = \frac{\gamma - 1}{M^2 - 1} \bullet \left[M^2 \bullet \left(EXw + \frac{dL}{\rho_a v_a} \right) - \left(MoX - \frac{dL}{\rho_a v_a} \right) / (\gamma - 1) \right] \tag{50}$$

$\frac{dT_a}{dz}$, $\frac{dv_a}{dz}$, and $\frac{dP}{dz}$ can be calculated from Eqs. (48), (49) and (50).

To validate this new method proposed in this paper, the temperatures calculated by the present method are compared with those reported by Zarling [23] in Fig. 5. As shown by Fig. 5, the variations of water temperature calculated by this new method are in good agreement with the results reported in [25]. The slight difference may be caused by different formulae used in two different methods (e.g. air/water viscosity, density conductivity et al.). It should be noticed that the mass flow ratio of water (L) to air (G_B) was set in that paper, but not by calculation. It can be seen that the temperature variation of sprayed water is strongly affected by the flow ratio, which is also stated at the beginning of this section.

4.3. Energy generated by turbines

The pressure difference between the air inside the tower and the outside is the integral of the product of the difference of the air densities by the gravity acceleration with respect to height:

$$\Delta P_{pot} = g \int_0^h (\rho_{z,\infty} - \rho_z) dz = g \int_0^h \rho_{z,\infty} dz - g \sum_0^h \rho_z \Delta h \tag{51}$$

where h is the tower height, $\rho_{z,\infty}$ and ρ_z are ambient air density and internal airflow density inside the tower at any height z, respectively. Although the air density in the tower changes along with the tower height, this change can be neglected as long as the Δh is small enough. In this paper, a proper value of 0.2 m is selected for Δh.

According to the International Standard Atmosphere [48], environment air temperature decreases with the altitude increasing. The temperature at altitude z meters above sea level is approximated by the following formula (only valid no more than ~18 km above Earth's surface):

$$T_{z,\infty} = T_{0,\infty} - T_{la} z \tag{52}$$

The pressure at altitude z is given by:

$$P_{z,\infty} = P_{0,\infty} \left(1 - \frac{T_{la} z}{T_{0,\infty}} \right)^{g/RT_{la}} \tag{53}$$

The density of air can be calculated according to the ideal gas law:

$$\rho_{z,\infty} = \rho_{0,\infty} \left(1 - \frac{T_{la} z}{T_{0,\infty}} \right)^{(g/RT_{la} - 1)} \tag{54}$$

where:

$P_{0,\infty}$ = sea-level standard atmospheric pressure, 101.325 kPa
$T_{0,\infty}$ = sea-level standard temperature, 288.15 K
T_{la} = temperature lapse rate, 0.0065 K/m
R = air specific constant, 287.05 J/(kg·K)

The specific potential energy due to heating is transformed to shaft power by turbines, frictional losses in the tower, and lost to the environment. The total pressure losses in the tower are the pressure potential minus ΔP_{turb} [49]:

$$\Delta P_{loss} = \Delta P_{pot} - \Delta P_{tur} = \Delta P_{pot} - \zeta \Delta P_{pot} \tag{55}$$

$$\Delta P_{loss} = \Delta P_{tur,in} + \Delta P_{br} + \Delta P_k \tag{56}$$

with

$$\Delta P_{tur,in} = \varepsilon_{tur,in} \bullet \frac{1}{2} \rho_{a,in} {v_{a,in}}^2 \tag{57}$$

$$\Delta P_{br} = \varepsilon_{br} \bullet \frac{1}{2} \rho_{a,in} {v_{a,in}}^2 \tag{58}$$

$$\Delta P_t = \varepsilon_t \bullet \frac{1}{2} \rho_{a,out} {v_{a,in}}^2 \tag{59}$$

$$\Delta P_k = \varepsilon_k \bullet \frac{1}{2} \rho_{a,out} {v_{a,out}}^2 \tag{60}$$

where ΔP_{turb} is the pressure drop at the turbine, ζ is the turbine pressure

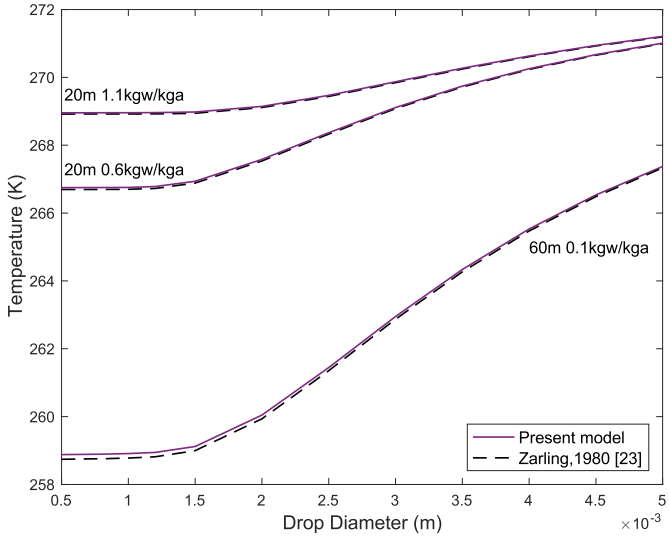

Fig. 5. The final temperature of a system of water droplets freezing process.

drop factor which is defined as the ratio of the pressure drop at the turbine to the total pressure potential. The ratio ζ is proposed to be 0.8 in [49], based on the previous work. In [49], the pressure losses are suggested as: $\Delta P_{turb,\ in}$ is the turbine inlet pressure loss with $\varepsilon_{turb,\ in} = 0.14$; ΔP_{br} is the pressure loss due to the internal bracing wheel (for strengthening the tower) drag forces with $\varepsilon_{br} = 0.25$; ΔP_k is the pressure loss due to exit kinetic energy loss with $\varepsilon_k = 1.26$. ΔP_t is the air collector-to-chimney (airflow from horizontal to vertical) transition section pressure loss with $\varepsilon_t = 0.268$ [45]. $v_{a,\ in}$ and $v_{a,\ out}$ represent the velocity of air at the inlet and outlet of the tower respectively.

According to [45], the airflow through the turbine can be treated as incompressible air, which is accurate enough for a practical purpose. This indicates that the difference in air density at the inlet and the outlet of the turbine can be neglected.

The power extracted from the turbine generators under a turbine load condition can be expressed as:

$$Pow_t = \eta \bullet \Delta P_{tur} \bullet S \bullet v_{a,in} \tag{61}$$

where η is the mechanical efficiency of the turbine generators, which is proposed to be 77% in [49].

5. Calculation procedure

The whole calculation process is divided into three steps:

Step 1: A guessed value for seawater quantity that the desalination system could handle was given firstly, to calculate the corresponding flow of the cold air flowing into the tower. The differential equations were calculated from the bottom of the tower to the top of it.

Step 2: As the mass of the cold air induced into the tower by the pressure difference is not known, a guessed value for cold air mass flow rate was given for the iteration process. The Runge-Kutta fourth-order method [50] was applied to solve the Eqs. (25), (26), (28), (48), (49) and (50) simultaneously for the upper part in the tower (before the phase change stage of the seawater). While for the lower (ice) part in the tower the Eqs. (26), (42), (43), (44) and the Eqs. (19)–(22) transformed from $\frac{dT_w}{dt}$ to $\frac{dT_w}{dz}$ need to be solved simultaneously. When these equations were solved, the temperature gradient against tower height was known. Then the mass of cold air can be calculated by Eqs. (51), (55) and (56). This value can be used as a reference value with the initial guessed value together to get a new G_B by Newton iteration method.

Step 3: This new G_B was used to recalculate the temperature variation of water droplets. If the water temperature on the top of the tower differed from the set temperature of 2 ° C, a new water mass flow rate would be suggested. This new water mass flow rate would be given to repeat step 1.

The final results would be obtained when the setting conditions were satisfied after steps 1 to 3. The whole calculation process is shown in Fig. 6.

6. Results and discussion

The experiments conducted by Gao [18,51] showed that more than 60% of impurity in the water was removed in the ice formed by the spray freezing. The ice was about 70% of the total volume of feed water, while the rest was separated by gravity and released as runoff. It was also demonstrated that a lower runoff fraction would deteriorate the rate of impurity reduction because more brine pocket would be entrapped in the ice powder. In another freeze desalination experiment [52], a mesh and a filter cloth were used for gravity filtration of an ice slurry (a mixture of 1 mm fine ice grains and brine, ice fraction is more than 70%). Approximately 60% of the total feed water was generated as the fresh water (at 0.5% NaCl concentration) after 50 min filtration. Although the salinity of the generated water could be further lowered by centrifugation, it is not discussed in this paper due to its energy consumption. From a conservative point, the ice fraction after the spray freezing process was set to be 70%, and 60% of the total feed water was assumed to be generated as fresh water. Thus, the final temperature of water droplets is set to be $-7.15°C$ based on Eq. (21). The initial

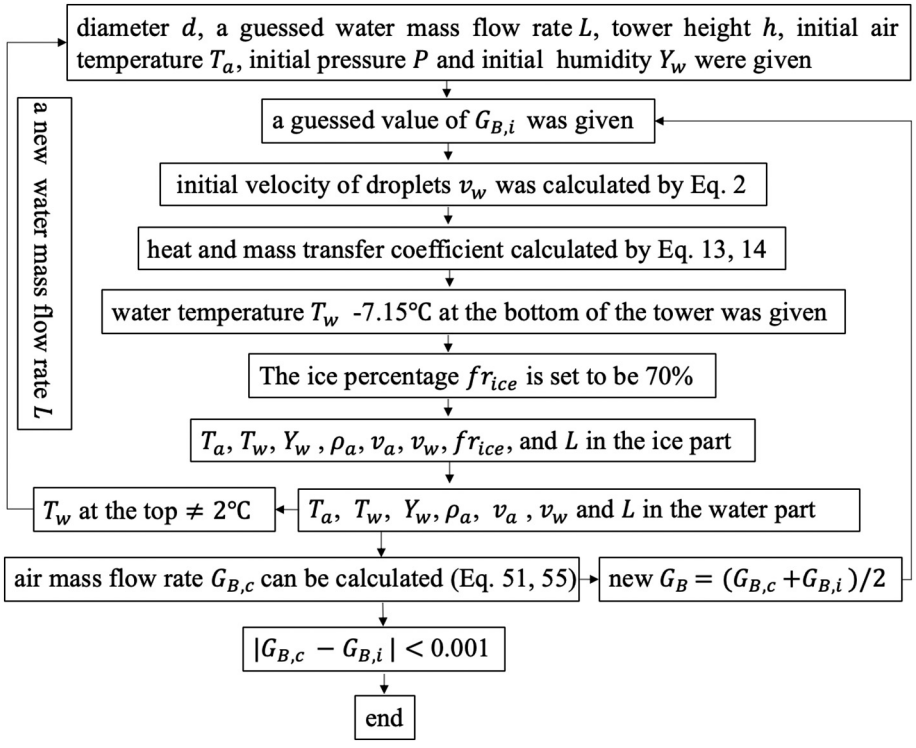

Fig. 6. The whole calculation process in this paper.

seawater temperature was set to be $2^{\circ}C$, and the relative humidity of the atmosphere was 80% [23].

6.1. Impact of environmental temperature on system performance

The atmospheric air temperature variation can greatly influence system performance. A spray freezing system with a $200m$ high tower under three different surrounding environmental temperatures is analyzed first. The 2 mm is chosen as the Sauter diameter of the water droplets sprayed in the tower. It is reasonable because more than 80% of the droplets had a diameter between 1 mm to 2.8 mm in the experiments conducted by Gao [18,51].

The variations of the water temperature are shown in Fig. 7. The typical atmospheric temperature in the cold regions discussed in references is $-26^{\circ}C$, $-18^{\circ}C$, and $-10^{\circ}C$ [17,23,30], those figures are also chosen in this paper. As stated above, the water temperature at the top of the tower is set to be $2^{\circ}C$ and it is set to be $-7.15^{\circ}C$ (70% ice fraction) at the bottom. The longer distance of the water required to reach the freezing point at $-26^{\circ}C$ is because of the larger mass flow ratio of feed water (L) to air (G_B) in that condition. More water needs longer distances to freeze when the air mass flow rate is smaller. The seawater requires a distance of 10.5 m, 8.3 m and 5.0 m to reach the freezing point at $-26^{\circ}C$, $-18^{\circ}C$, and $-10^{\circ}C$, respectively and the corresponding mass flow ratio of feed water to air is 0.089, 0.053, and 0.019, respectively (see Table 2). Although a higher mass flow rate of the water releases more heat to the air, more water droplets also hamper the airflow in the tower due to the drag forces between the water droplet and the air. Thus, the mass flow rate of the induced air would not increase proportionally with the increase of the water quantity.

When the ice is developed on the surface of the droplet, higher concentrated water remains inside the droplet, leading to the reduction of its freezing point. Thus, the temperature of the droplets continuously decreases until it reaches $7.15^{\circ}C$. The temperature decrease of water droplets is faster at $-26^{\circ}C$ at the lower half part of the tower (between the 0 m to about 100 m above the bottom) because of the large temperature difference between the cold air and water. At the height above 100 m, the change of water temperature becomes smooth due to the small temperature difference between the cold air and water.

The temperature and density variations of air in the tower are presented in Figs. 8 and 9, respectively. Figs. 8 and 9 show that a higher temperature difference between the air and water creates a higher heat transfer rate, a faster air temperature, and a higher rate of density change, especially during the lower half part of the tower. The final temperature of the air at the outlet of the tower is higher under the condition of the colder atmosphere, which is caused by a larger mass flow ratio of feed water (L) to air (G_B) in that condition. This feature is also reflected by the variations of density in Fig. 9. The final density of the air is 1.281, 1.288, and 1.293 kg/m^3 at the atmospheric temperature of $-26^{\circ}C$, $-18^{\circ}C$, and $-10^{\circ}C$, respectively. The corresponding final temperature of the outlet air (200 m above the bottom) is 267.7 K, 266.7 K, and 266.1K, respectively.

The main results of the freeze desalination system under different atmospheric temperatures are presented in Table 2. More air was induced into the tower to freeze the sprayed water droplets in the colder atmosphere, which generated more fresh water. At the same time more power was generated by the turbine. The maximum of the generated fresh water flow rate was 27.7 kg/s at a temperature of $-26^{\circ}C$. In this table, the fresh water generated was set to be 60% of the feed water and the mechanical efficiency of the pump for spray was set to be 0.85. The power consumption was calculated by $Pow_p = 0.85 m_w g h$. The third column was the result from the second column multiplied with the cross-section area S and the fresh water generation rate 60%.

6.2. Impact of droplets' diameter on system performance

The variations of droplets' diameters can also greatly influence system performance. In the following discussion, the temperature of the surrounding atmosphere is set to be $-18^{\circ}C$. The impact of droplets' diameters on air temperature and density is delineated in Figs. 10 and 11. As shown in Fig. 10, the air flows upwards from the bottom of the tower with a temperature rising. Compared to larger droplets, the temperature of air contacted with smaller droplets roses sharper at the beginning due to the larger area of heat transfer per unit mass. With the temperature difference between water and air being narrowed down quickly, the change of air temperature becomes slow and reaches a relatively “stable” state. This feature is also reflected by the variation of density in Fig. 11. The final density of the air is 1.265, 1.274, 1.288, 1.305 and 1.319 kg/m^3 with the diameter of 1, 1.5, 2, 2.5 and $3mm$, respectively. The corresponding final temperature of the outlet air (200 m above the bottom) is 270.9K, 269.5K, 266.7K, 263.4K and 260.5K, respectively. As discussed above, the final temperature of the outlet air would be higher when the droplets with smaller diameter sprayed into the tower, which is caused by the larger mass flow ratio of water to air (see Table 3).

The mass flow rate of the feed water that can be frozen by this system with different diameters of water droplets is present in Table 3. As expected, the water mass flow rate frozen by the system would be larger when smaller droplets sprayed into the tower because the smaller droplets have larger heat and mass transfer area per unit mass. Smaller droplets would also induce more air into the tower and generate more power. Though smaller droplets led to greater output (fresh water and power generated) compared to larger droplets, smaller droplets needed greater water pressure produced by the pump and were prone to jam in the sprinkler. Too small droplets may endure the risk of being blown out of the tower by the updraft air, which resulted in water loss. Those advantages and disadvantages of using smaller droplets should be traded off in a real project.

From Tables 2 and 3, it can be observed that the ratio of water mass flow rate to air mass flow rate was adjusted with the variation of the outside parameters. It cannot be set in this natural airflow induced by the pressure difference. The airflow rate is one of the most important factors that affect the fresh water output. The power generated by the air from turbines can compensate as large as one-third of the pump energy consumption, which was not recognized in previous research.

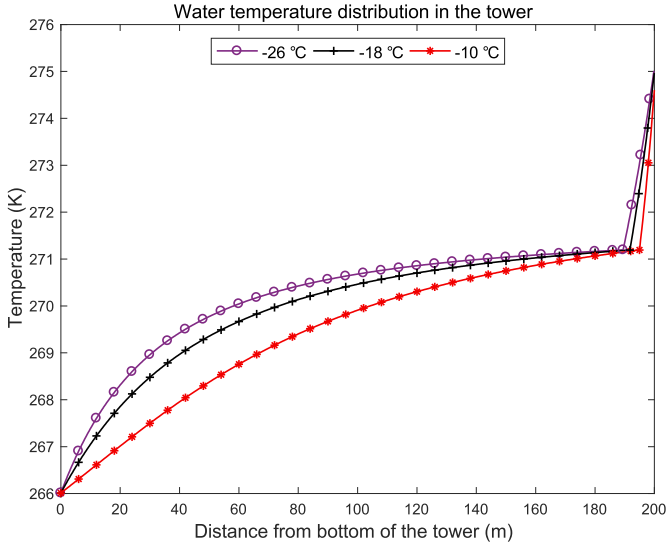

Fig. 7. The temperature variations of water droplets during the freezing process in the system.

Table 2
Results of the freeze desalination system under different atmospheric temperatures.

Temperature	Feed water flow rate ($kg/m^2 \cdot s$)	Fresh water generated (kg/s)	Airflow rate ($kg/m^2 \cdot s$)	Power generation/ consumption
$-26\ ^\circ C$	0.587	27.70	6.62	30.35%
$-18\ ^\circ C$	0.243	11.45	4.58	25.96%
$-10\ ^\circ C$	0.038	1.80	2.00	14.66%

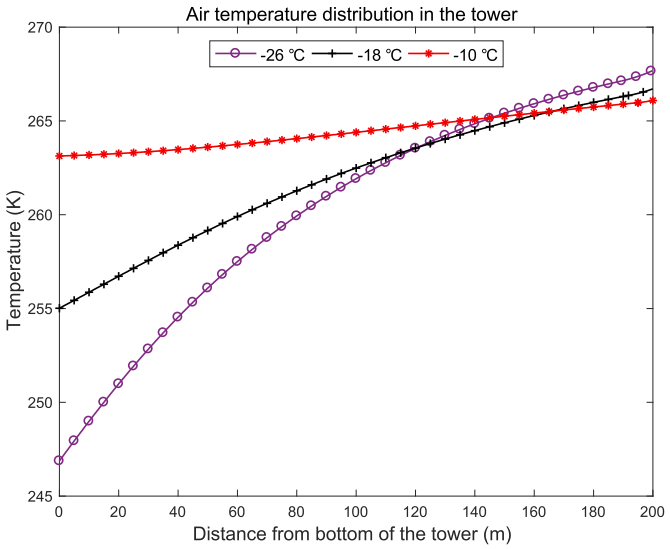

Fig. 8. The temperature variations of the induced air in the tower at different atmospheric temperatures.

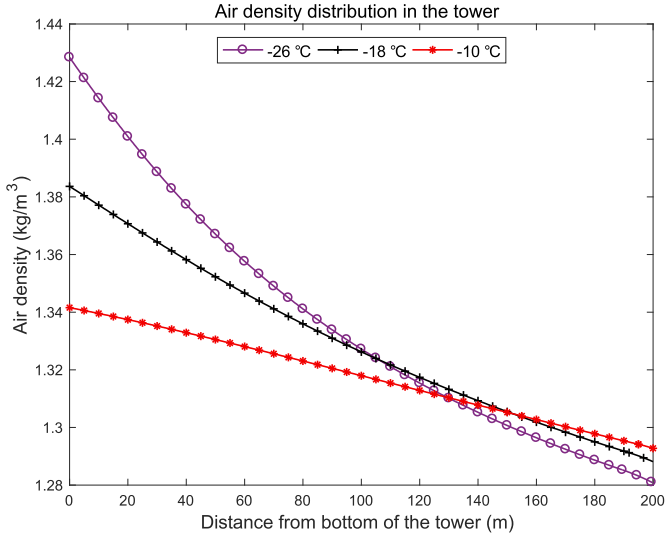

Fig. 9. The density variations of the induced air in the tower at different atmospheric temperatures.

6.3. Limitations

Although a new mathematical model has been developed for heat and mass transfer between compressible airflow and water droplets freezing in a tall tower, there were some limitations in this model which could be improved in further study. Firstly, the wind effects were not considered in this paper. Wind from the surrounding environment may significantly affect the performance. It may blow the hot air from the top of the tower down to the bottom. Secondly, in this study water droplets sprayed by nozzle were treated as a population of spherical uniform-size droplets. Actually, the droplets from the nozzle may not be in a uniform shape. The droplets collide and bounce with each other due to the different velocities. The turbulent flow of the air and the momentum transfer during the collision need to be analyzed further.

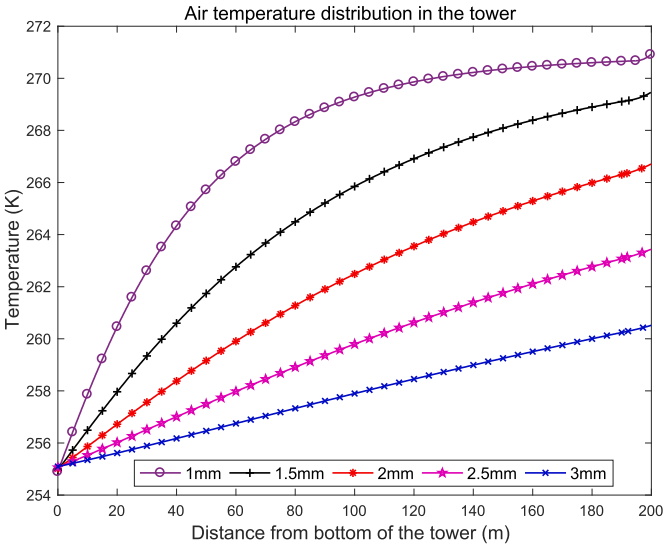

Fig. 10. The temperature variations of the induced air in the tower with different droplets' diameters.

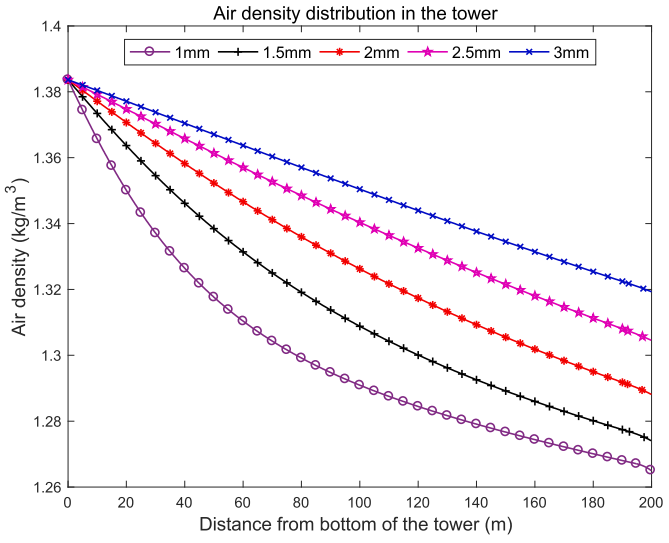

Fig. 11. The density variations of the induced air in the tower with different droplets' diameters.

Table 3
Results of the freeze desalination system with different diameters of water droplets.

Droplets diameter	Feed water flow rate ($kg/m^2 \cdot s$)	Fresh water generated (kg/s)	Airflow rate ($kg/m^2 \cdot s$)	Power generation/ consumption
$1mm$	0.436	20.54	6.14	34.85%
$1.5mm$	0.349	16.44	5.40	29.61%
$2mm$	0.243	11.45	4.58	25.96%
$2.5mm$	0.150	7.07	3.75	23.05%
$3mm$	0.084	3.96	2.96	20.23%

7. Economic analysis of this spray freeze desalination system

In this economic analysis, the case of water droplets with a diameter of 2 *mm* sprayed in the atmospheric temperature of $-26^{\circ}C$ was taken for comparison with other desalination methods in the following part.

Firstly, this new spray freeze desalination method needs lesser power consumption than some traditional methods. The power consumption required to produce 1 m^3 fresh water in this system is approximately 1.07 *kWh*, in which pump consumption is the major part of the operational energy cost. Considering the power generated by the turbines, this cost could be even lower by one third. If the altitude of the brackish water is above the height of the desalination system (e.g. the tailing water at a mine), a pipe could be made to channel the water to the tower and then benefit the operational cost of this freeze desalination system. In comparison, to produce 1 m^3 fresh water, a typical multi-stage flash distillation method needs 3.5 *kWh* power [53], the reverse osmosis method consumes 2–8 *kWh* power [7].

Secondly, this new spray freeze desalination method is more energy-efficient than other freeze desalination methods because of the high rate of heat and mass transfer between the water droplets and the air. A direct contact type seawater freeze desalination method was developed in [54]. In this experiment, a flow of refrigerant cooled by the cold energy from the regasification of LNG was injected into a seawater tank to generate ice. A technical and economic evaluation of this system was made by [55]. The optimum result of this system was that it generated 1.64 *kg/s* fresh water by consuming 7.83 *kg/s* seawater while the cold energy was provided by 1 *kg/s* LNG regasification (about 827 *kJ/kg* energy would be released by the LNG). Thus, the cold energy needed in this system was 504.3 *kJ* per kilogram fresh water. But in the new freezing system proposed in this paper, only 375.4 *kJ* cold energy (calculated from the enthalpy change of the airflow) was needed for generating 1 k of fresh water. A freezing crystallizer proposed by Attia et al. [56] needs 420 *kJ* energy and a disk column freezing crystallizer developed by Van der Ham et al. [15] needs 1037–1282 *kJ* energy to produce 1 *kg* fresh water. From this point, if there is free cold energy, the cold air (from the atmosphere or produced during the regasification of LNG) can be utilized in the desalination system proposed in this paper which is more energy-efficient than previous desalination systems discussed above.

Finally, according to the statistics data in [55], the price is about 1.5 USD for 1 m^3 freshwater and the industrial electricity price is about 0.15 USD for 1 *kWh* power. The total fresh water generated by this system is 873,547 m^3 per year under the assumption of no interruption of the free cold energy supply. The profit calculated by deduction between the fresh water income and the pump cost is about 1,179,288 USD per year (1,218,598 USD per year with power generated by the turbine). While the construction cost of a 200 m tower is about 5–10 million USD [57] depended on the location, labor force cost and the materials of the tower. Then the feedback period of this desalination system is about 4–8 years.

8. Conclusions

This paper investigated the feasibility of using spray freezing mechanism in a cold environment to desalinate seawater. Because of the low energy consumption, no need for huge pressure or membrane replacement work, and ignorable corrosion issues, freeze desalination is an attractive method to desalinate the seawater. While, the spray freezing method in this paper is more energy-efficient than the block, layer or falling film freeze processes because it has higher heat and mass transfer area per unit seawater and lower heat resistance.

In this paper, the freezing character of a freely falling seawater droplet was analyzed first. The freezing process of a droplet was divided by several stages, the heat and mass transfer of the droplet in each stage was investigated. An improved mathematical method was proposed to numerically simulate this freezing process. Then the heat, momentum, and mass transfer between a system of water droplets sprayed in the desalination system and the natural convective airflow induced by the hot water were studied. An iterative process to solve the proposed differential equations was introduced in this paper.

The results demonstrated the seawater desalination capacity was affected by the surrounding atmospheric temperature and the diameter of the water droplets. Colder atmospheric temperature and smaller droplets produce more fresh water. The 200 m high desalination system could generate 27.7 *kg/s* fresh water (at 0.5% NaCl concentration) with the 2 mm diameter of the sprayed water droplet in the atmospheric temperature of $-26^{\circ}C$. The induced natural convective airflow could generate one-third of the energy consumption of the water pump in this system, while this free energy was never respected in previous research.

This new spray freeze desalination method consumes lesser power. The power consumption required to produce 1 m^3 fresh water in this system is about 1.07 *kWh*. With consideration of the power generated by the wind turbines, this cost could be even lower by one third. Compared with some traditional desalination methods, the newly proposed spray freeze desalination method consumes less power while the same mass flow rate of fresh water is generated. This new method is also energy efficient compared to other freeze desalination approach because of the direct contact between the cold and warm flow (low heat resistance) and the large area of heat and mass transfer per unit mass of water. It needs only 375.4 *kJ* cold energy to produce one-kilogram fresh water.

The spray freeze desalination process can generate fresh water and produce green power simultaneously. It deserves to be considered by the desalination industry due to its high efficiency if free cold energy is available. The economic analysis of the system in different countries needs further study based on the local water, labor, electricity and land prices in the next step.

CRediT authorship contribution statement

Yang Liu: Data curation, Writing- Original draft preparation, Software.

Tingzhen Ming: Supervision, Conceptualization, Methodology.

Yongjia Wu: Validation, Investigation.

Renaud de Richter: Conceptualization, Writing- Reviewing.

Yueping Fang: Visualization, Writing- Reviewing and Editing.

Nan Zhou: Writing- Reviewing and Editing.

Declaration of competing interest

The authors declare that they have no known competing financial interests or personal relationships that could have appeared to influence the work reported in this paper.

Acknowledgements

This study is financially supported by the National Natural Science Foundation of China (Grant No. 51778511), the Hubei Provincial Natural Science Foundation of China (Grant No. 2018CFA029), the Key Project of ESI Discipline Development of Wuhan University of Technology (WUT Grant No. 2017001), the Fundamental Research Funds for the Central Universities (WUT Grant No. 2019IVB082), and the Scientific Research Foundation of Wuhan University of Technology (No. 40120237).

References

[1] M.o.W. Resources, Water resources in China, http://www.mwr.gov.cn/english/mainsubjects/201604/P020160406508110938538.pdf, (2019).

[2] H.R. Peyton, P.R. Johnson, C.E. Behlke, Saline Conversion and Ice Structures From Artificially Grown Sea Ice, University of Alaska, Arctic Environmental Engineering Laboratory and University of Alaska, Institute of Water Resources, 1967.

[3] J. Chang, J. Zuo, K.-J. Lu, T.-S. Chung, Freeze desalination of seawater using LNG cold energy, Water Res. 102 (2016) 282–293.
[4] P.M. Williams, M. Ahmad, B.S. Connolly, D.L. Oatley-Radcliffe, Technology for freeze concentration in the desalination industry, Desalination 356 (2015) 314–327.
[5] K. El Kadi, I. Janajreh, Desalination by freeze crystallization: an overview, The International Journal of Thermal & Environmental Engineering (IJTEE) 15 (2017) 103–110.
[6] G. Naidu, X. Zhong, S. Vigneswaran, Comparison of membrane distillation and freeze crystallizer as alternatives for reverse osmosis concentrate treatment, Desalination 427 (2018) 10–18.
[7] P. Byrne, L. Fournaison, A. Delahaye, Y. Ait Oumeziane, L. Serres, P. Loulergue, et al., A review on the coupling of cooling, desalination and solar photovoltaic systems, Renew. Sust. Energ. Rev. 47 (2015) 703–717.
[8] H. Yang, M. Fu, Z. Zhan, R. Wang, Y. Jiang, Study on combined freezing-based desalination processes with microwave treatment, Desalination 475 (2020) 114201.
[9] H. Shin, B. Kalista, S. Jeong, A. Jang, Optimization of simplified freeze desalination with surface scraped freeze crystallizer for producing irrigation water without seeding, Desalination 452 (2019) 68–74.
[10] W. Tang, J. Tao, J.-a. Wang, C. Liu, H. Zhang, Sea ice desalination under gravity using microwave heating, Desalination 430 (2018) 159–164.
[11] W. Cao, C. Beggs, I.M. Mujtaba, Theoretical approach of freeze seawater desalination on flake ice maker utilizing LNG cold energy, Desalination 355 (2015) 22–32.
[12] P. Wang, T.S. Chung, A conceptual demonstration of freeze desalination-membrane distillation (FD-MD) hybrid desalination process utilizing liquefied natural gas (LNG) cold energy, Water Res. 46 (2012) 4037–4052.
[13] M. John, A. Häkkinen, M. Louhi-Kultanen, Purification efficiency of natural freeze crystallization for urban wastewaters, Cold Reg. Sci. Technol. 170 (2020) 102953.
[14] F. van der Ham, G.J. Witkamp, J. de Graauw, G.M. van Rosmalen, Eutectic freeze crystallization simultaneous formation and separation of two solid phases, J. Cryst. Growth 198-199 (1999) 744–748.
[15] F. van der Ham, G.J. Witkamp, J. de Graauw, G.M. van Rosmalen, Eutectic freeze crystallization: application to process streams and waste water purification, Chem. Eng. Process. Process Intensif. 37 (1998) 207–213.
[16] W. Gao, D.W. Smith, D.C. Sego, Freezing behavior of freely suspended industrial wastewater droplets, Cold Reg. Sci. Technol. 31 (2000) 13–26.
[17] K.R. Sultana, K. Pope, L.S. Lam, Y.S. Muzychka, Phase change and droplet dynamics for a free falling water droplet, Int. J. Heat Mass Transf. 115 (2017) 461–470.
[18] W. Gao, D.W. Smith, D.C. Sego, Treatment of pulp mill and oil sands industrial wastewaters by the partial spray freezing process, Water Res. 38 (2004) 579–584.
[19] K.W. Biggar, R. Donahue, D. Sego, M. Johnson, S. Birch, Spray freezing decontamination of tailings water at the Colomac Mine, Cold Reg. Sci. Technol. 42 (2005) 106–119.
[20] C. Tatarniuk, R. Donahue, D. Sego, Freeze separation of salt contaminated melt water and sand wash water at snow storage and sand recycling facilities, Cold Reg. Sci. Technol. 57 (2009) 61–66.
[21] J.r. Schlaich, R. Bergermann, W. Schiel, G. Weinrebe, Design of commercial solar updraft tower systems—utilization of solar induced convective flows for power generation, Journal of Solar Energy Engineering 127 (2005) 117–124.
[22] M.M. Conde, M. Rovere, P. Gallo, Molecular dynamics simulations of freezing-point depression of TIP4P/2005 water in solution with NaCl, J. Mol. Liq. 261 (2018) 513–519.
[23] A.R. Dehghani-Sanij, S. MacLachlan, G.F. Naterer, Y.S. Muzychka, R.D. Haynes, V. Enjilela, Multistage cooling and freezing of a saline spherical water droplet, Int. J. Therm. Sci. 147 (2020) 106095.
[24] O.J. González Pedraza, J.J. Pacheco Ibarra, C. Rubio-Maya, S.R. Galván González, J.A. Rangel Arista, Numerical study of the drift and evaporation of water droplets cooled down by a forced stream of air, Appl. Therm. Eng. 142 (2018) 292–302.
[25] J.P. Zarling, Heat and Mass Transfer From Freely Falling Drops at Low Temperatures, (1980), p. 20.
[26] H. Cui, N. Li, J. Peng, J. Cheng, N. Zhang, Z. Wu, Modeling the particle scavenging and thermal efficiencies of a heat absorbing scrubber, Build. Environ. 111 (2017) 218–227.
[27] IOC, SCOR, IAPSO, The International Thermodynamic Equation Of Seawater – 2010: Calculation and Use of Thermodynamic Properties, Intergovernmental Oceanographic Commission, 2010, p. 196.
[28] M. Llano-Restrepo, R. Monsalve-Reyes, Modeling and simulation of counterflow wet-cooling towers and the accurate calculation and correlation of mass transfer coefficients for thermal performance prediction, Int. J. Refrig. 74 (2017) 47–72.
[29] R.a.A.C.E. American Society of Heating, Inc, ASHRAE Handbook—Fundamentals, N.E., Atlanta, (2013).
[30] A.R. Dehghani-Sanij, Y.S. Muzychka, G.F. Naterer, Droplet trajectory and thermal analysis of impinging saline spray flow on marine platforms in cold seas and ocean regions, Ocean Eng. 148 (2018) 538–547.
[31] M.N. Chowdhury, F.Y. Testik, M.C. Hornack, A.A. Khan, Free fall of water drops in laboratory rainfall simulations, Atmos. Res. 168 (2016) 158–168.
[32] J.O. Laws, Measurements of the fall-velocity of water-drops and raindrops, EOS Trans. Am. Geophys. Union 22 (1941) 709–721.
[33] R. Gunn, G.D. Kinzer, The terminal velocity of fall for water droplets in stagnant air, J. Meteorol. 6 (1949) 243–248.
[34] P.K. Wang, H.R. Pruppacher, Acceleration to terminal velocity of cloud and raindrops, J. Appl. Meteorol. 16 (1977) 275–280.
[35] S.-C. Yao, V.E. Schrock, Heat and mass transfer from freely falling drops, J. Heat Transf. 98 (1976) 120–126.
[36] J.P. Hindmarsh, A.B. Russell, X.D. Chen, Experimental and numerical analysis of the temperature transition of a suspended freezing water droplet, Int. J. Heat Mass Transf. 46 (2003) 1199–1213.
[37] J.P. Hindmarsh, A.B. Russell, X.D. Chen, Experimental and numerical analysis of the temperature transition of a freezing food solution droplet, Chem. Eng. Sci. 59 (2004) 2503–2515.
[38] W.E. Ranz, W.R. Marshall Jr., Evaporation From Drops—I–II, (1952).
[39] I.B. Sebastião, B. Bhatnagar, S. Tchessalov, S. Ohtake, M. Plitzko, B. Luy, et al., Bulk dynamic spray freeze-drying part 1: modeling of droplet cooling and phase change, J. Pharm. Sci. 108 (2019) 2063–2074.
[40] I.B. Sebastião, B. Bhatnagar, S. Tchessalov, S. Ohtake, M. Plitzko, B. Luy, et al., Bulk dynamic spray freeze-drying part 2: model-based parametric study for spray-freezing process characterization, J. Pharm. Sci. 108 (2019) 2075–2085.
[41] S. Hassid, I. Merksamer, R. Guetta, Energy towers – the effect of droplet coalescence on power and the environment, Sol. Energy 86 (2012) 1443–1453.
[42] N. Makkinejad, Temperature profile in countercurrent/cocurrent spray towers, Int. J. Heat Mass Transf. 44 (2001) 14.
[43] T.W. von Backström, A.J. Gannon, Compressible flow through solar power plant chimneys, Journal of Solar Energy Engineering 122 (2000) 138.
[44] X. Zhou, J. Yang, B. Xiao, G. Hou, Y. Wu, Numerical investigation of a compressible flow through a solar chimney, Heat Transfer Engineering 30 (2009) 670–676.
[45] A.S. Ćoćić, V.D. Djordjević, One-dimensional analysis of compressible flow in solar chimney power plants, Sol. Energy 135 (2016) 810–820.
[46] M. Lucas, P.J. Martínez, J. Ruiz, A.S. Kaiser, A. Viedma, On the influence of psychrometric ambient conditions on cooling tower drift deposition, Int. J. Heat Mass Transf. 53 (2010) 594–604.
[47] Y.A. Çengel, A.J. Ghajar, Heat and Mass Transfer: Fundamentals & Applications, McGraw-Hill, Fifth ed, 2015.
[48] Standard Atmosphere, International Organization for Standardization, 1975.
[49] X. Zhou, Y. Xu, S. Yuan, R. Chen, B. Song, Pressure and power potential of sloped-collector solar updraft tower power plant, Int. J. Heat Mass Transf. 75 (2014) 450–461.
[50] S.C. Chapra, Applied Numerical Methods With Matlab for Engineers, Third edition, McGraw-Hill, New York, 2012.
[51] W. Gao, D.W. Smith, D.C. Sego, Spray freezing treatment of water from oil sands tailing ponds, J. Environ. Eng. Sci. 2 (2003).
[52] D. Chen, C. Zhang, H. Rong, C. Wei, S. Gou, Experimental study on seawater desalination through supercooled water dynamic ice making, Desalination 476 (2020) 114233.
[53] Y. Zheng, K.B. Hatzell, Technoeconomic analysis of solar thermal desalination, Desalination 474 (2020) 114168.
[54] C. Xie, L. Zhang, Y. Liu, Q. Lv, G. Ruan, S.S. Hosseini, A direct contact type ice generator for seawater freezing desalination using LNG cold energy, Desalination 435 (2018) 293–300.
[55] C.-W. Ong, C.-L. Chen, Technical and economic evaluation of seawater freezing desalination using liquefied natural gas, Energy 181 (2019).
[56] A.A.A. Attia, New proposed system for freeze water desalination using auto reversed R-22 vapor compression heat pump, Desalination 254 (2010) 179–184.
[57] A. Ayoub, B. Gjorgiev, G. Sansavini, Cooling towers performance in a changing climate: techno-economic modeling and design optimization, Energy 160 (2018) 1133–1143.